The Astrophysical Journal, 935:158 (13pp), 2022 August 20 https://doi.org/10.3847/1538-4357/ac7f32

Exploring Refractory Organics in Extraterrestrial Particles

Alexey Potapov[1], Maria Elisabetta Palumbo[2], Zelia Dionnet[3], Andrea Longobardo[4,5], Cornelia Jäger[1], Giuseppe Baratta[2], Alessandra Rotundi[4,5], and Thomas Henning[6]

[1] Laboratory Astrophysics Group of the Max Planck Institute for Astronomy at the Friedrich Schiller University Jena, Institute of Solid State Physics, Helmholtzweg 3, D-07743 Jena, Germany; alexey.potapov@uni-jena.de
[2] INAF-Osservatorio Astrofisico di Catania, Via Santa Sofia 78, I-95123 Catania, Italy
[3] Université Paris-Saclay, CNRS, Institut d'Astrophysique Spatiale, F-91405, Orsay, France
[4] Dip. Scienze e Tecnologie, Università degli Studi di Napoli "Parthenope," Centro Direzionale I C4, I-80143 Napoli, Italy
[5] INAF-Istituto di Astrofisica e Planetologia Spaziali, Via Fosso del Cavaliere 100, I-00133 Roma, Italy
[6] Max Planck Institute for Astronomy, Königstuhl 17, D-69117 Heidelberg, Germany
Received 2021 December 1; revised 2022 July 1; accepted 2022 July 5; published 2022 August 23

Abstract

The origin of organic compounds detected in meteorites and comets, some of which could have served as precursors of life on Earth, remains an open question. The aim of the present study is to make one more step in revealing the nature and composition of organic materials of extraterrestrial particles by comparing infrared spectra of laboratory-made refractory organic residues to spectra of cometary particles returned by the Stardust mission, interplanetary dust particles, and meteorites. Our results reinforce the idea of a pathway for the formation of refractory organics through energetic and thermal processing of molecular ices in the solar nebula. There is also the possibility that some of the organic material had formed already in the parental molecular cloud before it entered the solar nebula. The majority of the IR "organic" bands of the studied extraterrestrial particles can be reproduced in the spectra of the laboratory organic residues. We confirm the detection of water, nitriles, hydrocarbons, and carbonates in extraterrestrial particles and link it to the formation location of the particles in the outer regions of the solar nebula. To clarify the genesis of the species, high-sensitivity observations in combination with laboratory measurements like those presented in this paper are needed. Thus, this study presents one more piece of the puzzle of the origin of water and organic compounds on Earth and motivation for future collaborative laboratory and observational projects.

Unified Astronomy Thesaurus concepts: Astrochemistry (75); Solar system (1528); Laboratory astrophysics (2004); Meteorite composition (1037); Comet origins (2203)

1. Introduction

One of the main hypotheses about the source of organic compounds that could serve as the basis of life on Earth is their formation in the parental molecular cloud or the protoplanetary disk and delivery to Earth through extraterrestrial objects (Oro 1961; Cronin & Chang 1993; Brack 1999; Pearce et al. 2017). Asteroids, interplanetary dust particles (IDPs), and, to some extent, comets bombarded intensively the surface of early Earth and could have contributed directly with their organic content to the formation of a terrestrial prebiotic world (Chyba & Sagan 1992).

Organic compounds, which are critical for life as we know it, such as ribose, amino acids, and nucleobases, have been detected in meteorites and comets (Cronin & Chang 1993; Elsila et al. 2009; Cobb & Pudritz 2014; Altwegg et al. 2016) and synthesized in laboratory experiments simulating the evolution of icy dust grains in the interstellar medium (ISM; Bernstein et al. 2002; Muñoz Caro et al. 2002; Nuevo et al. 2006; Elsila et al. 2007; Nuevo et al. 2012; Meinert et al. 2016; Oba et al. 2016; Krasnokutski et al. 2020) and circumstellar disks around young stars (Potapov et al. 2022). Moreover, meteorites, comets, and IDPs contain refractory organic compounds (Cooper et al. 2001; Matrajt et al. 2004; Keller et al. 2006; Rotundi et al. 2008; Dartois et al. 2013; Rotundi et al. 2014; Goesmann et al. 2015; Dartois et al. 2018; Dionnet et al. 2018). Such compounds may be reproduced in laboratory experiments by gas-phase condensation of amorphous carbon-based materials (Colangeli et al. 1995; Hammer et al. 2000; Fanchini et al. 2002; Rodil 2005; Jäger et al. 2008; Quirico et al. 2008) and by UV or ion irradiation of molecular ices containing C-, H-, O-, and N-bearing molecules, such as H_2O, CO, N_2, CO_2, NH_3, CH_4, and CH_3OH (the most abundant ice species observed in astrophysical environments and comets), and their subsequent heating to room temperature leading to the formation of refractory organic residues (Munoz Caro & Schutte 2003; Palumbo et al. 2004; Fresneau et al. 2017; Accolla et al. 2018; Poch et al. 2020; Potapov et al. 2021).

The origin of the organic compounds detected in meteorites, comets, and IDPs remains an open question. The main issues are their amount, chemical pathways, formation conditions (including formation location in the solar nebula), and alteration by chemical processing within the nebula. Answering these questions will help not only to reveal the astrochemical heritage of the solar system but also to draw a more complete picture of the physicochemical processes in interstellar and circumstellar media due to their common link (Ehrenfreund & Charnley 2000; Caselli & Ceccarelli 2012; Henning & Semenov 2013; Sandford et al. 2020).

In order to identify components of primitive bodies and dust grains in the solar system and to constrain the origin and evolution of refractory organics inside extraterrestrial matter, it is critical to compare analogs obtained in the laboratory with extraterrestrial samples collected on Earth, or directly in space thanks to sample return missions. Similarities in optical and structural properties and chemical compositions of extraterrestrial and laboratory-synthesized materials have been shown. However, a direct comparison of the spectra of real cosmic particles and their analogs is relatively rare. A perfect example of such a comparison is the assignment of the 3.2 μm feature in the spectrum of the comet 67P/Churyumov–Gerasimenko to ammonium salts produced in the laboratory (Poch et al. 2020). Ultracarbonaceous Antarctic micrometeorites exhibit IR signatures that are similar to those observed in laboratory-synthesized carbon-based materials and organic residues (Dartois et al. 2013; Baratta et al. 2015; Accolla et al. 2018; Dartois et al. 2018). It was also suggested that interstellar ices should lead to organic materials enriched in heteroatoms that present similarities with cometary materials but strongly differ from meteoritic organic materials (Fresneau et al. 2017).

This study presents a comparison of the IR spectra of laboratory-made refractory organic residues produced by UV or ion irradiation of simple molecular ices and their subsequent heating to room temperature to the spectra of cometary particles returned by the Stardust mission (hereafter, Stardust particles), IDPs, and meteorites. Our aim is to make one more step in revealing the nature and composition of organic materials of extraterrestrial particles.

2. Methods

2.1. Extraterrestrial Particles and Their Spectral Measurements

In this section, we present the extraterrestrial samples chosen as a point of reference for comparison with analogs: (i) two meteoritic fragments, (ii) two IDPs, and (iii) three cometary particles collected by the Stardust mission.

We selected two very different samples of carbonaceous chondrites: (i) the Paris meteorite (petrologic type: CM2.7–2.8), as it is one of the least altered carbonaceous chondrites available in the laboratory (Hewins et al. 2014), and (ii) a fragment of the Northwest Africa (NWA) 5515 meteorite, a CK4 chondrite representative of meteorites that has undergone thermal metamorphism. Our aim was to compare the laboratory samples with two meteoritic samples with very different types of alteration. The classification of meteorite types is presented elsewhere (Rubin et al. 2007). IR measurements of the Paris meteorite were performed in transmission on a fragment ($50 \times 40 \times 3$ μm^3) crushed inside diamond windows. An Agilent (model Cary 670/620) microspectrometer, with its internal source (Globar), and a 25× objective, installed on the SMIS (Spectroscopy and Microscopy in the Infrared Using Synchrotron) beamline of the SOLEIL synchrotron (France), was used to obtain data in the spectral range 4000–800 cm^{-1} with a resolution of 4 cm^{-1}. The sample's average spectrum is used here. A complete analysis of this sample is presented elsewhere (Dionnet et al. 2018). The spectrum of NWA 5515 was collected on a 3D grain with the same setup (Aléon-Toppani et al. 2021).

The spectra of IDPs were another point of comparison for the laboratory analogs. The sample L2021C5 was crushed in diamond windows and its IR transmission spectrum was measured at the SMIS beamline of the SOLEIL synchrotron with a NicPlan microscope, coupled to a Magna 860 FTIR spectrometer (Thermo Fisher) operating in transmission in the 5000–650 cm^{-1} range and with a resolution of 4 cm^{-1}. A complete analysis of the particle is presented elsewhere (Brunetto et al. 2011). The U217B19 IR spectrum has been presented and analyzed by Ishii et al. (2018). The IR data were provided by Hope Ishii.

Then, we compared the analogs' spectra with those of Stardust particles directly collected in the coma of the comet 81P/Wild and brought back to Earth in 2006. Collected samples were trapped in aerogel. A few of them were analyzed thanks to IR spectroscopy (Rotundi et al. 2008), namely particles 35.17 (size 10×7 μm^2), 35.21 (size 20×13 μm^2), and 35.26 (size 11×19 μm^2). Particles 35.17, 35.21, and 35.26 were deposited on a KBr window and then IR data were collected. Particle 35.17 was studied in transmission by the LANDS team at Laboratorio di Fisica Cosmica e Planetologia (LFCP), Napoli, with a microscope attached to an FTIR interferometer (model Bruker Equinox-55), in the range 7000–600 cm^{-1} and a spectral resolution of 4 cm^{-1}. In contrast, the spectra of particles 35.21 and 35.26 were measured in reflection by the Orsay-IAS group using a NicPlan microscope associated with a Magma 860 FTIR spectrometer equipped with MCT detectors, in the range 4000–650 cm^{-1} and with a spectral resolution of 4 cm^{-1}. Correction of the Stardust particles' spectra was applied by subtraction of the normalized spectra of the aerogel, measured in the surrounding pixels.

Concerning the Stardust samples, the organic contribution of the aerogel was removed from the spectra. For each particle, a spectrum of the surrounding aerogel was taken and then subtracted. Water was more of a challenge. The samples could contain small amounts of adsorbed water due to air measurements and conservation of the samples. Concerning the IDPs, some of them were put inside silicone oil, but they were cleaned with hexane, which should remove contamination. It is possible that there were small remains for the bands around 1281–1257 and 1261–1259 cm^{-1} (7.81–7.96 and 7.93–7.94 μm). Many analyses have been done on the organic matter of IDPs with such a protocol (for instance, Merouane et al. 2014).

2.2. Experiments in Jena

Residues formed after UV irradiation of simple ices deposited onto silicate grains were obtained by the Laboratory Astrophysics Group of the Max Planck Institute for Astronomy (Germany).

The experimental setup and procedure have been presented in two recent papers devoted to dust/ice mixtures (Potapov et al. 2018a, 2018b). In brief, nanometer-sized amorphous $MgSiO_3$ silicate grains were produced by laser ablation of a Mg:Si (1:1) target in a quenching atmosphere of 4 Torr O_2. After the formation, the grains were extracted through a nozzle and a skimmer from the ablation chamber and deposited onto KBr substrates at a temperature of 10 K and a pressure in the deposition chamber of 5×10^{-8} mbar. Grains interact on a substrate forming a porous layer of fractal aggregates with sizes of up to several tens of nanometers (Jäger et al. 2008; Sabri et al. 2014). The thickness of the grain deposits was controlled by a quartz crystal resonator microbalance using known values for the deposit area of 1 cm^2 and for the density of 2.5 g cm^{-3} and was about 150 nm.

Ice mixtures CH_3OH:H_2O, CH_3OH:H_2O:NH_3, CO_2:H_2O:NH_3, and CH_4:H_2O:NH_3 containing C-, N-, and H-bearing ice molecules abundant in astrophysical environments (Boogert et al. 2015) with volume ratios of about 1 for $MgSiO_3$/C-bearing molecule and 10 for C-bearing molecule/H_2O and C-bearing molecule/NH_3 were deposited on the silicate grains. The initial molecular compositions of the ices were chosen to address the efficient formation of refractory organic residues. The

H_2O, CO_2, CH_4, NH_3, and CH_3OH ices' thicknesses were calculated from their vibrational bands at 3250, 2342, 3009, 1073, and 1026 cm^{-1} using band strengths of 2.0×10^{-16} (Gerakines et al. 1995), 7.6×10^{-17} (Gerakines et al. 1995), 5.7×10^{-18} (Hudgins et al. 1993), 1.7×10^{-17} (d'Hendecourt & Allamandola 1986), and 1.8×10^{-17} cm molecule^{-1} (Hudgins et al. 1993) correspondingly. The deposition time in all experiments was about 15 minutes.

After deposition, the silicate/ice mixtures were irradiated for 6 hr by a broadband deuterium lamp (L11798, Hamamatsu) with a flux of 10^{15} photons cm^{-2} s^{-1}. Thus, the final fluence was about 2×10^{19} photons cm^{-2}. The lamp had a broad spectrum from 400 to 118 nm with the main peaks at 160 nm (7.7 eV) and at about 122 nm (10.2 eV) corresponding to the emission of molecular and atomic hydrogen. After irradiation, the cooling was stopped and the samples were warmed up to room temperature. IR spectra of the samples at room temperature were taken in situ using an FTIR spectrometer (Vertex 80v, Bruker) in the transmission mode at a resolution of 1 cm^{-1}. The spectra of pure KBr substrates recorded at room temperature before the depositions and irradiation experiments were used as reference spectra.

2.3. Experiments in Catania

Residues formed after ion irradiation of simple ices were obtained in the Laboratory for Experimental Astrophysics at INAF-Osservatorio Astrofisico di Catania (Italy). The spectra of the residues have been already presented in a previous study (Accolla et al. 2018).

Gas mixtures were prepared in a mixing chamber and admitted into an ultrahigh-vacuum (UHV) chamber ($P < 10^{-9}$ mbar) through a needle valve. Inside the chamber, the gas condensed on a cold KBr substrate (17 K) in thermal contact with the cold finger of a closed-cycle He cryostat.

The UHV chamber was interfaced with a 200 kV ion implanter (Danfysik 1080–200). The thickness of the ice samples was measured during accretion by a laser interference technique. After deposition, each ice sample was irradiated with 200 keV H^+. After ion irradiation, the sample was warmed up to room temperature.

During irradiation, the ion current was kept below 1 μA cm^{-2}. The dose (in units of eV/16u, where u is the unified atomic mass unit defined as 1/12 of the mass of an isolated atom of carbon-12) was obtained from knowledge of the fluence (that was measured during the experiment, in units of ions cm^{-2}) and the stopping power (that was obtained by SRIM software in units of eV cm^2 per molecule) as the thickness of the ice sample was lower than the penetration depth of 200 keV protons. For the spectra presented in this work the dose was 120 eV/16u (CH_4:CO = 1:1), 126 eV/16u (N_2:CH_4 = 1:1), 106 eV/16u (N_2:CH_4:CO = 1:1:1), and 122 eV/16u (N_2:CH_4:H_2O = 1:1:1). The initial ice molecular composition was chosen to optimize the formation of the corresponding refractory organic residue.

The vacuum chamber was placed in the sample compartment of an FTIR spectrometer (Vertex 70, Bruker). Transmission IR spectra were taken through KBr windows in the chamber and a hole in the cold finger before ice deposition (background spectrum), after deposition, after each step of ion irradiation, at selected temperature values during warm-up, and at room temperature. The spectra of the residues shown in this work were taken at room temperature the day after the irradiation, without breaking the vacuum. The spectra were taken at a resolution of 1 cm^{-1} and a sampling of 0.25 cm^{-1}. The sample holder formed an angle of 45° with the IR beam and the ion beam. As a consequence, IR transmission spectra could be taken at each experimental step without rotating the sample. More details on the experimental setup and procedure can be found elsewhere (Urso et al. 2016; Accolla et al. 2018).

3. Results

Vacuum UV (VUV) photons or ions cause carbonization processes of ices that lead to the formation of refractory materials. Depending on the irradiation dose, these materials can be partly or completely refractory corresponding to partly soluble or insoluble organic matter. The best analog of the samples produced in our experiments is kerogen. The nature of kerogen is not well defined. Its disordered structure can be described as a mixture of aromatic and aliphatic subunits containing a large number of functional groups. It is now well accepted that the refractory organic materials in cometary dust as well as in meteorites are dominated by high molecular weight organic components very similar to kerogen-like materials (Osawa et al. 2009; Matthewman et al. 2013; Wooden et al. 2017).

The IR absorption spectra of the samples obtained after UV or ion irradiation of molecular ices and subsequent heating to room temperature are presented in Figure 1.

Comparison of low-temperature spectra before and after energetic processing is outside of the scope of the present study. Examples of such a comparison can be found in the literature (Islam et al. 2014; Munoz Caro et al. 2019). The ice mixtures used for the production of laboratory organic residues, the detected IR bands of the residues, and their attributions are listed in Tables 1 and 2.

All residue spectra show similar profiles containing bands that can be attributed to the vibration modes of different refractory organic materials (additionally, the Si–O stretching band around 1000 cm^{-1} in Jena samples containing amorphous $MgSiO_3$ grains). When an N-bearing species (N_2 or NH_3) is present in the original ice mixture, a broad feature at about 2200 cm^{-1} (4.54 μm) is observed in the spectra of the residues (see Figure 1 and Tables 1 and 2). This feature is assigned to nitriles and isonitriles (C $\equiv$ N triple bond; Accolla et al. 2018). From a qualitative point of view, the spectra of the laboratory samples are very similar to each other. The similarity is due to the fact that the organic residues have the same functional groups, such as OH and NH stretching vibrations; CH_3, CH_2, C = O, C = C, and C = N stretching vibrations; N–H and CH bending vibrations; and so on. The majority of the observed IR features have the same or slightly shifted band positions (see Tables 1 and 2). The spectral bands not present in both data sets are the following:

1. The silicate band at 1040 cm^{-1} (9.62 μm) in the Jena spectra due to the presence of $MgSiO_3$ grains.
2. The weak bands at about 1515 and 1430 cm^{-1} (6.58 and 6.99 μm) in the Jena spectra attributed to $CO_3{}^{2-}$ stretching in magnesium carbonates ($MgCO_3$).
3. The bands at 1628 and 1580 cm^{-1} (6.14 and 6.33 μm) in the Catania spectra, which can be attributed to C = C and/or C = N stretching. In combination with the more intense and broad C $\equiv$ N 2200 cm^{-1} band (as compared to the Jena samples), this result points to the more

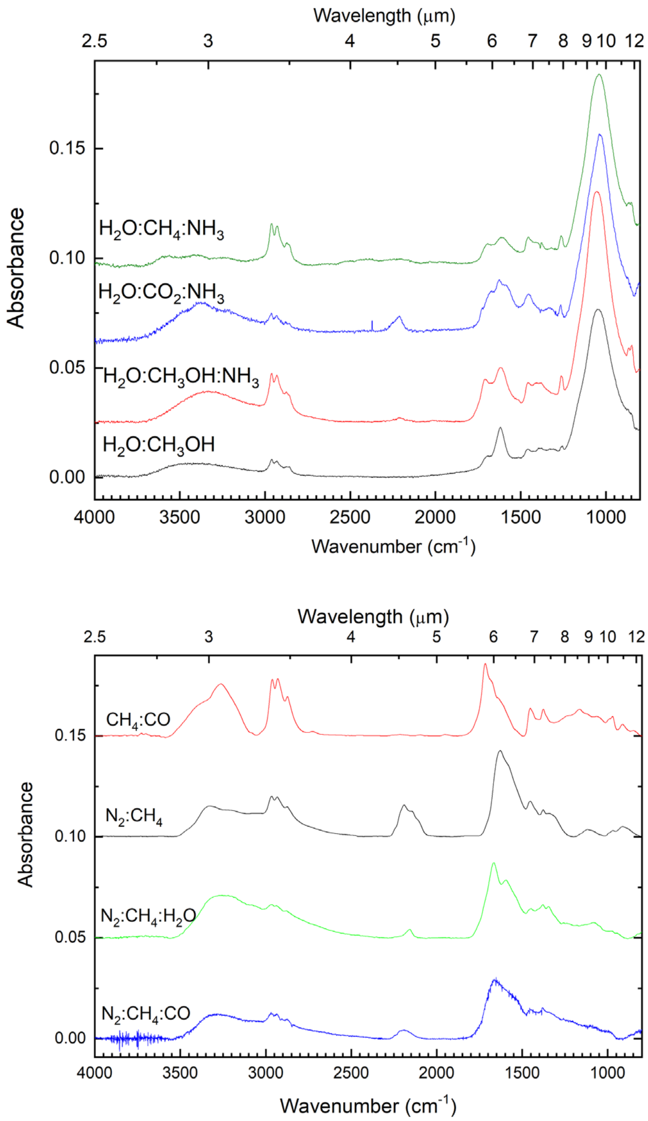

Figure 1. The IR absorption spectra of the laboratory organic residues. Upper: Produced in Jena on the surface of silicate grains by UV irradiation of different ice mixtures (mentioned in the figure) at 10 K and subsequent heating of the samples up to room temperature. Lower: Produced in Catania on KBr substrates by ion irradiation of different ice mixtures (mentioned in the figure) at 17 K and subsequent heating of the samples up to room temperature. The spectra are vertically shifted for clarity.

efficient formation of N-bearing residues by ion irradiation of N_2-containing ices.

4. A number of bands without attributions in both spectral sets.
5. In addition, the bands ranging from about 1650 to 1720 cm^{-1} (6.06–5.81 μm) in the Catania samples are broader and show different shapes compared to those in the Jena samples. This might point to the presence of N–H bending vibrations in addition to C = O or C = N groups caused by the presence of $–NH_2$ groups in the ion-irradiated samples (Bernstein et al. 1995; Krasnokutski et al. 2022; Oba et al. 2022). However, a clear identification of the functional groups and composition of the processed organics based on the IR spectra is difficult. Additional analytical characterization methods such as mass spectrometry, X-ray photoelectron spectroscopy, and X-ray absorption near-edge structure (XANES) are required.

A detailed study on the reproducibility and stability of the residues produced after ion irradiation of icy samples in Catania has been reported (Baratta et al. 2015; Accolla et al. 2018; Baratta et al. 2019). In particular, 30 residues have been produced after ion irradiation of icy samples made of N_2:CH_4:CO = 1:1:1 deposited at 17 K (Baratta et al. 2015). Icy samples of three different thicknesses have been irradiated at the same ion dose (110 ± 5 eV/16u). It has been shown that the thickness of the final residue is proportional to the thickness of the initial ice sample and that the profile and relative intensity of IR bands do not depend on the sample thickness. Furthermore, the stability of the residues has been checked over a period of about 1200 days (Baratta et al. 2019). It has been found that the intensity of the –C ≡ N feature at about 2190 cm^{-1} (4.57 μm) decreases in the beginning and then stabilizes after 200 days and does not vary further, within uncertainties, after 700 days. No significant variations have been observed for the other IR bands.

The experiments on the UV irradiation of ices did not produce completely reproducible results. The ice mixtures produced in Jena were irradiated with VUV photons for 6 hr. Under these conditions, the carbonization process of the ices was well advanced leading to the formation of a kerogen-like material. This has been proven by ex situ analysis of the residues (C. Jäger et al., in preparation). Analyses performed by high-resolution transmission electron microscopy, energy-dispersive X-ray spectroscopy, and electron energy loss spectroscopy have shown that the content of C, O, and N can vary in the nanometer scale within one sample. In our samples, a number of functional groups such as ≡CH, $=CH_2$, $–CH_3$, C = O, HC = O, –COOH, and NH_x, as well as ether and ester groups, are formed. However, the ratios of these functional groups can differ as well as the carbon structure in the nanometer scale, but the general trend of the formation of O- and N-bearing groups is the same. We have to note that IR spectroscopy is not sensitive enough to detect small changes in the kerogen-like carbon structure.

In the following, we present the results of the comparison of the IR spectra of meteorites (primitive carbonaceous chondrites), IDPs, and Stardust particles to the spectra of organic residues produced in the laboratory. The spectra of the residues produced from N-free and N-containing ice mixtures are quite similar except for the C ≡ N feature around 2200 cm^{-1} (4.54 μm); that is why only the spectra for the N-containing mixtures are shown in the next three figures.

We compared the laboratory spectra with the spectra of meteoritic samples, namely the Paris meteorite and the NWA 5515 meteorite. Figure 2 shows the comparison of the absorption spectra of the meteorites and laboratory organic residues. The detected IR bands and their attributions for the meteorites are presented in Table 3.

As the analogs described in this paper are made from molecular ices, it is very relevant to compare their spectra with cometary ones. IDPs are derived from a larger variety of small bodies compared to macroscopic meteorites (Sandford & Bradley 1989; Bradley 2003); in particular, chondritic porous aggregate IDPs come potentially from comets (Mackinnon & Rietmeijer 1987). Thus, we used the spectra of the IDP U217B19 and the IDP L2021C5 as another point of comparison to the laboratory analogs. The comparison is presented in Figure 3. The detected IR bands and their attributions for the IDPs are presented in Table 3.

Table 1
IR Bands (cm^{-1}) of the Jena Samples and Their Attributions

$CH_3OH:H_2O$	$CH_3OH:H_2O:NH_3$	$CO_2:H_2O:NH_3$	$CH_4:H_2O:NH_3$	Band Attributions
3750–3000	3750–3000	3750–3000	3750–3000	OH stretching, NH stretching (Munoz Caro & Schutte 2003)
2962, 2932	2962, 2932	2962, 2932	2962, 2930	CH stretching (asym; Colangeli et al. 1995)
2876, 2858	2875, 2859	2879, 2859	2872, 2858	CH stretching (sym; Colangeli et al. 1995)
...	...	...	2523	?
...	...	...	2410	?
...	...	2371, 2365	...	?
...	2260–2175	2290–2155	2325–2096	C ≡ N stretching (Accolla et al. 2018)
1697, 1618	1707, 1615	1715, 1622	1697, 1610	C = O, C = C, C = N stretching (Munoz Caro & Schutte 2003), HOH bending, NH_2 bending (Accolla et al. 2018)
1513	1512	1516	1515	CO_3^{2-} stretching (Aguiar et al. 2009; Ciaravella et al. 2018)
1458	1458	1455	1455	CH bending (Munoz Caro & Schutte 2003)
1427	...	...	1432	CO_3^{2-} stretching (Aguiar et al. 2009; Ciaravella et al. 2018)
1394, 1377	1380	...	...	CH bending (sym; Colangeli et al. 1995; Jäger et al. 2008)
1330	1330	1334	1320	COO^- stretching (sym; Munoz Caro & Schutte 2003)
1300	...	...	1300	?
1263, 1255	1263, 1257	1265	1263, 1258	?
1040	1040	1040	1040	SiO stretching
860	865, 847	...	865, 850	out-of-plane CH bending (Colangeli et al. 1995; Jäger et al. 2008)
...	804	804	804	?

Then, we compared the spectra of the laboratory samples with those of particles directly collected in the coma of a comet. Indeed, thanks to the Stardust mission, thousands of particles with a diameter between 3 and 2000 μm were collected in the coma of the comet 81P/Wild and brought back to Earth in 2006 (Sandford 2007). Figure 4 shows the result of the comparison of the spectra of three Stardust particles and the laboratory organic residues. The detected IR bands and their attributions for the Stardust particles are presented in Table 4.

Several previous experimental investigations have focused on the formation of organic residues after UV photolysis and ion bombardment of ice mixtures (Bernstein et al. 1995; Greenberg et al. 1995; Munoz Caro & Schutte 2003; Ferini et al. 2004; Palumbo et al. 2004; Kobayashi et al. 2008; Materese et al. 2014; Baratta et al. 2015; Oba et al. 2016; Tachibana et al. 2017; Accolla et al. 2018; Urso et al. 2020). Most of these studies are based on the analysis of samples by IR spectroscopy. This is a very powerful, nondestructive, and well-consolidated analytical technique; however, it has the disadvantage of the IR bands of various functional groups occurring at about the same wavelengths independently of the structure and composition of the material. To overcome this limit several studies have coupled a second technique to IR spectroscopy. As an example, high-performance liquid chromatography (Kobayashi et al. 2008; Oba et al. 2019), gas chromatography–mass spectrometry (Materese et al. 2014), optical microscopy (Tachibana et al. 2017), X-ray photoelectron spectroscopy (Accolla et al. 2018), XANES (Materese et al. 2014), high-resolution mass spectrometry (Oba et al. 2019), and very high-resolution mass spectrometry (Urso et al. 2020) have been used. The combination of different analytical techniques allows a deeper knowledge of the sample and a better comprehension of its chemical and physical properties. As has been pointed out, relevant complex molecules in organic refractory residues have a very low abundance and have been identified by gas chromatography–mass spectroscopy, while they are difficult or even impossible to identify by IR spectroscopy (Hudson et al. 2008). In addition, after comparing results obtained on residues produced by UV photolysis and ion irradiation of different ice mixtures, Hudson et al. (2008) suggested that energetic processing of almost any ice mixture containing C, H, N, and O atoms probably results in the formation of amino acid precursors that, if hydrolyzed, give rise to amino acids themselves. Similar conclusions have been drawn in Materese et al. (2014).

However, IR spectroscopy remains the most suitable technique for a direct comparison with remote astronomical observations and for laboratory analysis of extraterrestrial samples. In most of the studies mentioned above the initial ice mixtures were composed of H_2O, CH_3OH or CH_4 as the C-bearing species, and N_2 or NH_3 as the N-bearing species. In particular, NH_3 was used when residue was formed after UV photolysis. In fact, as discussed in Kobayashi et al. (2008) and Islam et al. (2014) after UV photolysis of N_2-containing mixtures the formation efficiency of molecular species that include nitrogen is about two orders of magnitude lower than the value observed after ion irradiation. The results presented in these studies confirm that a refractory organic residue is efficiently formed after ion irradiation and UV photolysis of ice samples as long as a C-bearing species is present in the initial

Table 2
IR Bands (cm^{-1}) of the Catania Samples and Their Attributions

CH_4:CO	N_2:CH_4	N_2:CH_4:CO	N_2:CH_4:H_2O	Band Attributions
3500–3000	3500–3000	3500–3000	3500–3000	OH stretching, NH stretching (Munoz Caro & Schutte 2003)
2961, 2930	2966, 2933	2966, 2934	2966, 2934	CH stretching (asym; Colangeli et al. 1995)
2873	2873	2873	2877	CH stretching (sym; Colangeli et al. 1995)
...	2270–2050	2270–2050	2270–2050	C ≡ N stretching (Accolla et al. 2018)
1716, 1628	1628, 1580	1662	1666, 1660	C = O, C = C, C = N stretching (Munoz Caro & Schutte 2003) HOH bending, NH_2 bending (Accolla et al. 2018)
1454	1453	1452	1450	CH bending (Munoz Caro & Schutte 2003)
1376	1378	1379	1380	CH deform. (sym; Colangeli et al. 1995; Jäger et al. 2008)
...	1320	1340	1348	COO^- stretching (sym; Munoz Caro & Schutte 2003)
1240	...	1260	1240	?
1161	...	...	...	?
...	1100	1095	1085	?
1057	...	...	...	?
990	...	990	...	?
970	970	...	970	?
...	...	...	940	?
911	911	...	...	?
850	...	...	...	out-of-plane CH bending (Colangeli et al. 1995; Jäger et al. 2008)

ice mixture. However, as pointed out in Urso et al. (2020) the detailed chemical and physical properties of the residue depend on the initial ice mixture and on the irradiation dose. These findings support the ongoing effort to perform a systematic study of the chemical and physical properties of residues as a function of different parameters such as the initial ice mixture and the irradiation dose (R. G. Urso et al., in preparation).

All extraterrestrial particles of our study (meteorites, IDPs, and cometary particles) present mixtures of organic components and minerals, and both have proper signatures in the IR spectra. The silicate features are the most prominent in the spectra. As one can see from the comparisons presented in Figures 2–4 and from Tables 1–4, the majority of the IR bands caused by the presence of organic materials in the studied particles can be reproduced in the spectra of the laboratory analogs. However, the spectra of the particles and the spectra of the residues do not match perfectly. This is not surprising as we consider a very limited number of ice mixtures with only a few molecular species and with particular abundance ratios. On one hand, none of these ice mixtures is exactly equal to the expected chemical composition of ice grain mantles or ice surfaces of solar system bodies. On the other hand, we have considered mixtures made of molecules that have been observed or are expected to be present in astrophysical ices. Quantitative differences between the laboratory spectra clearly defined by the initial ice mixture, type, energy, and conditions of the processing are observed and, if studied systematically, will clarify the genesis of the extraterrestrial organic materials. Below, we discuss a few important results that have been obtained in our study.

The broad band is observed in the spectra of all extraterrestrial particles in the range of 3750–3000 cm^{-1} (2.67–3.33 μm). For Stardust particle 3517 the range is a bit narrower, 3600–3000 cm^{-1} (2.78–3.33 μm); however, it can be a baseline problem. For Stardust particle 3526 the band is split into two. The band is observed in the same range in the spectra of the Jena samples. It has been previously shown by the Jena group that some water molecules mixed with silicates at low temperatures are trapped on silicate grains beyond the desorption temperature of water ice (Potapov et al. 2018a, 2018b, 2021). Trapped water presenting, probably, water molecules strongly bound in hydrophilic binding sites on silicate grains shows up as weak OH stretching and OH bending bands in the 3600 and 1600 cm^{-1} (2.78 and 6.25 μm) spectral regions correspondingly, as is observed in this study for the Jena samples. For the Catania samples, the band is narrower, 3500–3000 cm^{-1} (2.86–3.33 μm). As far as it was also detected in "oxygenless" samples, it was mainly attributed to the –NH_2 and –NH groups; additionally, it was attributed to the –OH functional groups in the case of O-containing ices (Accolla et al. 2018). Comparing the two sets of samples, Jena and Catania, we can clearly attribute the spectral range 3750–3500 cm^{-1} (2.67–2.86 μm) to the OH stretching of water molecules trapped on silicate grains and the spectral range 3500–3000 cm^{-1} (2.86–3.33 μm) to both NH and OH groups in the residue. Note that a contribution from OH groups in alcohols is also possible in these spectral ranges.

The band located between 2300 and 2000 cm^{-1} (4.35 and 5.0 μm) related to the C ≡ N triple bond is detected in the spectra of both IDPs and of Stardust particles 3521 and 3526 and is not detected in the meteorites. The detection of this

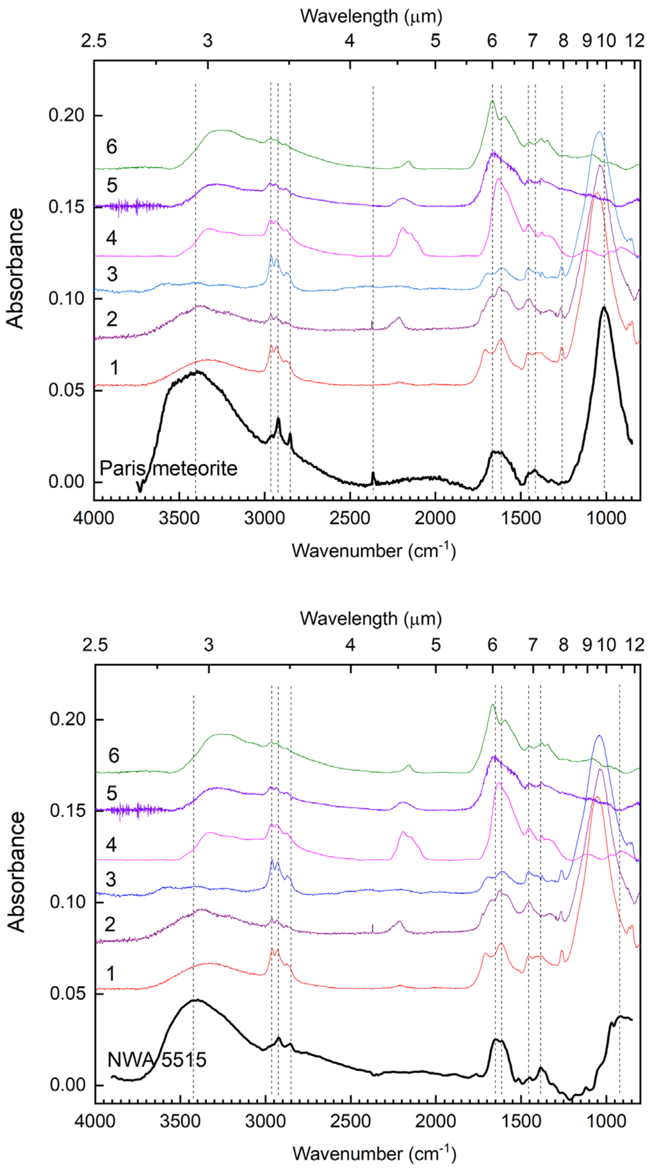

Figure 2. Comparison of the absorption IR spectra of the Paris (upper) and NWA 5515 (lower) meteorites and the laboratory organic residues produced in Jena and Catania from N-containing ice mixtures (mentioned in the figure). The spectra are vertically shifted for clarity. The vertical dashed lines indicate the most prominent absorption features in the meteorite spectra. Ice mixtures: (1) H_2O:CH_3OH:NH_3 (UV irradiation, Jena), (2) H_2O:CO_2:NH_3 (UV irradiation, Jena), (3) H_2O:CH_4:NH_3 (UV irradiation, Jena), (4) N_2:CH_4 (ion irradiation, Catania), (5) N_2:CH_4:CO (ion irradiation, Catania), and (6) N_2:CH_4:H_2O (ion irradiation, Catania).

feature in extraterrestrial particles is an important result meaning that N-bearing species were present in the particle material at the formation of the organic residue.

In the spectra of the extraterrestrial particles (both meteorites, IDP L2021C5, and Stardust particle 3517), we see evidence of the presence of organic carbonates with IR signatures between 1410–1430 and 1520–1540 cm^{-1} (between ∼7.0 and ∼6.5 μm). Furthermore, a set of organic signatures is present in the spectra of the extraterrestrial particles and their analogs: CH_2 and CH_3 aliphatic stretching bands, localized respectively around 2930 cm^{-1} and 2960 cm^{-1} (3.41 and 3.38 μm) for the asymmetric vibration and around 2850 cm^{-1} and 2870 cm^{-1} (3.51 and 3.48 μm) for the symmetric vibration; a C = O stretching band (around 1700 cm^{-1}, 5.88 μm); C = C and C = N stretching bands (around 1630 and 1580 cm^{-1}, 6.13 and 6.33 μm); and CH bending bands (around 1460, 1380, 1260 and 850 cm^{-1}; 6.85, 7.25, 7.94 and 11.76 μm). However, their attributions to definite species (if possible) need an additional structural and elementary analysis, which is outside of the scope of the present study.

Most of the extraterrestrial samples presented in this study (Paris and NWA 5515 meteorites, IDP L2021C5, and Stardust particle 3521) show a broad silicate band with a maximum between 930 and 1045 cm^{-1} (10.75 and 9.57 μm). The variation of the maximum could be due to compositional or structural differences. For instance, primitive meteorites, such as Paris, showing a matrix with partly amorphous hydrated silicates will present a maximum above 1000 cm^{-1} (10 μm). In contrast, NWA 5515 is a more heated meteorite and exhibits a spectral signature around 930 cm^{-1} (10.75 μm), which corresponds to a matrix rich in anhydrous phases. Conversely, some samples exhibit a silicate signature composed of several peaks, such as particle 3526. This sample is mainly composed of crystalline olivine (bands at 1017 and 871 cm^{-1}, 9.83 and 11.48 μm) (Rotundi et al. 2008). Indeed, complex structures of the silicate band in the spectra of the extraterrestrial particles suggest crystalline silicates. In the cases of the Paris meteorite and the IDP L2021C5 presenting more amorphous silicates, we observe a good coincidence with the silicate band in the spectra of the Jena samples. In the case of the Stardust particles, the profile of the silicate band is due to the contribution given by the silicate in the particle as well as by the silica aerogel, in which each particle has been embedded. Thus, in this case, the comparison with laboratory analogs is not straightforward.

4. Discussion

4.1 Pathways to Refractory Organics

The similarities between the spectra of the laboratory samples and the extraterrestrial particles reinforce the idea of a pathway for the formation of refractory organics through energetic and thermal processing of molecular ices in the solar nebula or in its parent molecular cloud. Ion irradiation and UV photolysis of ice mixtures could significantly contribute to the formation of the organic matter observed in extraterrestrial particles. Of course, this does not exclude the assumption that other processes are at work as well. The laboratory spectra of the samples produced by UV or ion processing are qualitatively very similar to each other. This allows us to make the conclusion that the formation of an organic residue is a general result independent of the initial mixture (as far as C-bearing species are included) and of the type of energetic processing. The same conclusion was reached in a number of previous studies (Islam et al. 2014; Munoz Caro et al. 2014). Slight differences in the composition and structure of the residues depend on the initial mixture, the type of energetic processing, and the photon or ion fluence. This was also demonstrated in studies of organic residues of different ice mixtures after VUV processing (Bernstein et al. 1995; Greenberg et al. 1995).

Below, we compare the ion and UV fluxes and doses in different astrophysical environments (see also Table 5) and their possible effects on interstellar and circumstellar ices. It has been estimated that in dense molecular clouds the effective 1 MeV proton flux of cosmic ions is 1 cm^{-2} s^{-1} (Mennella et al. 2003) and the UV flux, due to the cosmic-ray-induced

Table 3
IR Bands (cm^{-1}) of Paris and NWA 5515 Meteorites and IDPs U217B19 and L2021C5 and Their Attributions

Paris Meteorite	NWA Meteorite	IDP U217B19	IDP L2021C5	Band Attributions
3730–3000 (p)	3750–3000 (p)	3800–3000 (p)	3700–3000 (p)	OH stretching, NH stretching (Munoz Caro & Schutte 2003)
2958 (p), 2920 (p)	2963 (p), 2925 (p)	2957, 2921 (p)	2957 (p), 2922 (p)	CH stretching (asym; Colangeli et al. 1995)
2851 (p)	2850 (p)	...	2870, 2854 (p)	CH stretching (sym; Colangeli et al. 1995)
2366 (p)	...	...	...	?
...	...	2320–2090 (p)	2240–2151 (p)	C ≡ N stretching (Accolla et al. 2018)
...	...	1920 (p)	...	?
1662 (p), 1611 (p)	1650 (p), 1613 (p)	1664 (p), 1595 (p)	1604 (p)	C = O, C = C, C = N stretching (Munoz Caro & Schutte 2003) HOH bending, NH_2 bending (Accolla et al. 2018)
...	1515	...	1515	CO_3^{2-} stretching (Aguiar et al. 2009; Ciaravella et al. 2018)
1454 (p)	1449 (p)	1450 (p)	1461 (p)	CH bending (Munoz Caro & Schutte 2003)
1418 (p)	...	...	1415 (p)	CO_3^{2-} stretching (Aguiar et al. 2009; Ciaravella et al. 2018)
...	1385 (p)	...	1378	CH bending (sym; Colangeli et al. 1995; Jäger et al. 2008)
...	1358	1356 (p)	...	?
1320	1312	...	1322	COO^- stretching (sym; Munoz Caro & Schutte 2003)
1260 (p)	1258	1247	1261 (p)	?
...	1181	1166	...	?
...	1120	...	...	?
1020 (p)	930 (p)	1095 (p)	945 (p)	SiO stretching
...	...	840 (p)	...	out-of-plane CH bending (Colangeli et al. 1995; Jäger et al. 2008)

Note. The band positions are determined in this study. The notation (p) indicates the most prominent absorption features shown in Figures 2 and 3.

emission of molecular hydrogen, is of the order of 2×10^3 – 3×10^4 photons cm^{-2} s^{-1}, depending on the assumed cosmic-ray spectrum at low energy (Prasad & Tarafdar 1983; Shen et al. 2004). As estimated by Shen et al. (2004), after 10^7 yr the dose deposited by cosmic rays on water ice grain mantles varies within the range of 1–10 eV/molecule, and the dose deposited by UV photons varies within the range of 10–100 eV/molecule. Based on these results, the energy input by UV photons is about an order of magnitude higher than the energy input by cosmic-ray particles.

Moore (1999) showed that in diffuse regions of the ISM UV photons deposit more energy in icy mantles than 1 MeV protons. In particular, after 10^7 yr the dose deposited by UV photons is of the order of 10^6 eV/molecule and the dose deposited by low-energy cosmic rays is on the order of 30 eV/molecule. It should be noted that icy grain mantles are not observed in diffuse regions. This is ascribed to the fact that the photon-induced desorption rate is higher than the gas adsorption rate (Westley et al. 1995). However, evidence of the presence of solid-state water (similar to the trapped water discussed in this study) in the diffuse ISM has been provided recently by Potapov et al. (2021) on the basis of the combination of laboratory data and infrared observations.

Pedersen & Gomez de Castro (2011) have modeled the protoplanetary disk of a young stellar object assuming that the UV radiation field of a T Tauri star at 500 au from the central object is 2.9×10^{10} photons cm^{-2} s^{-1}. Strazzulla et al. (1983) have estimated that the flux of 1 MeV protons in a T Tauri star is 2×10^{10} cm^{-2} s^{-1} at 1 au. Assuming that the flux decreases with distance as d^{-2}, at 500 au the value is 8×10^4 cm^{-2} s^{-1}.

With regard to the solar system, it has been estimated that near the cometary surface in the Oort cloud the dose deposited by cosmic rays after 10^9 yr is as high as hundreds of eV/16u, where u is the unified atomic mass unit defined as 1/12 of the mass of an isolated atom of carbon-12 (Strazzulla & Johnson 1991; Modica et al. 2012). Stellar UV fluxes for Sun-like stars have been estimated in the range of 10^{11} photons cm^{-2} s^{-1} at 1 au to 10^7 photons cm^{-2} s^{-1} at 100 au (T. Löhne, private communication). Assuming that the flux decreases with distance as d^{-2}, this gives us 10^5–10^3 photons cm^{-2} s^{-1} at 10^3–10^4 au.

Thus, the dose of UV photons irradiating ice grain mantles in the ISM and planet-forming disks is orders of magnitude higher than that of energetic ions. On the other hand, UV photons are absorbed in the outermost layers, on the order of 10^2 nm (Cruz-Diaz et al. 2014a, 2014b), depending on the optical constants of the target material (Baratta et al. 2002). Thus, their effects would be important for small grains and surface processes and would be negligible for large bodies with respect to the effects caused by energetic ions, which can penetrate as deep as a few meters (Strazzulla & Johnson 1991; Modica et al. 2012). In addition, the effects of UV photons would be important if NH_3 (and not N_2) is the main N-bearing species in icy grain mantles. If N_2 is the main N-bearing species in interstellar and circumstellar ices, UV photons compared to ions would produce negligible chemical effects due to the very low

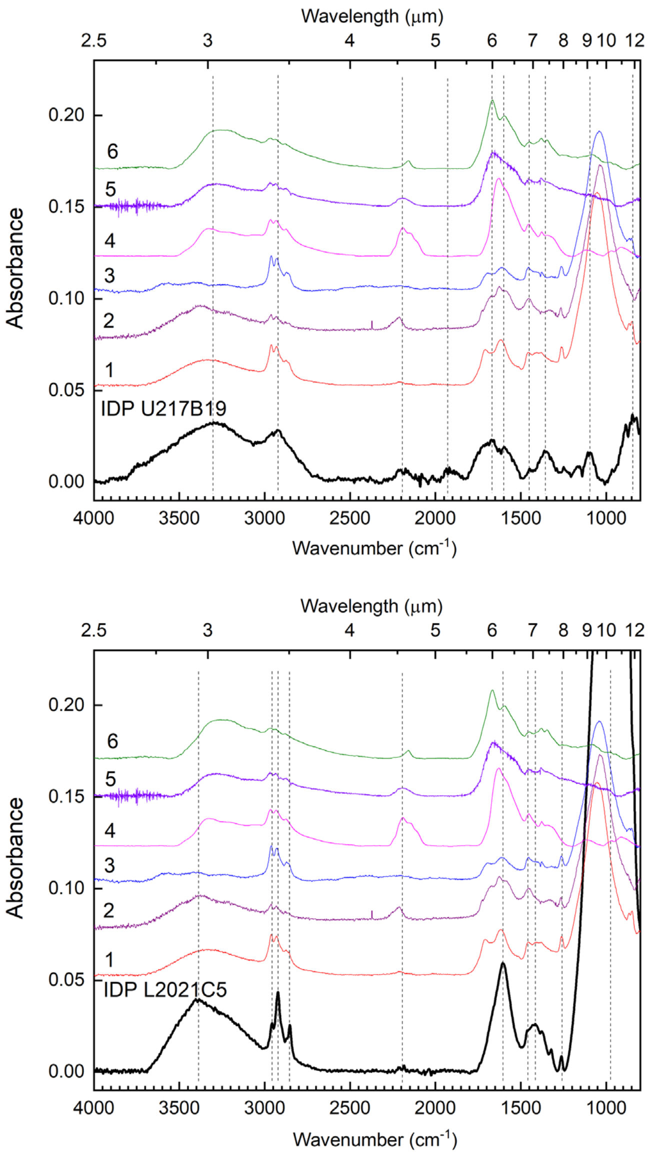

Figure 3. Comparison of the IR absorption spectra of the IDP U217B19 (upper) and the IDP L2021C5 (lower) and the laboratory organic residues produced in Jena and Catania from N-containing ice mixtures (mentioned in the figure). The spectra are vertically shifted for clarity. The original spectrum of the IDP U217B19 is multiplied by 10. The vertical dashed lines indicate the most prominent absorption features in the IDPs' spectra. Ice mixtures: (1) H_2O:CH_3OH:NH_3 (UV irradiation, Jena), (2) H_2O:CO_2:NH_3 (UV irradiation, Jena), (3) H_2O:CH_4:NH_3 (UV irradiation, Jena), (4) N_2:CH_4 (ion irradiation, Catania), (5) N_2:CH_4:CO (ion irradiation, Catania), and (6) N_2:CH_4:H_2O (ion irradiation, Catania).

absorption of UV light by N_2 (Hudson & Moore 2002; Kobayashi et al. 2008; Wu et al. 2012; Islam et al. 2014).

Ion irradiation experiments have been intentionally performed in order to reach a dose of the order of 100 eV/16u because this dose is able to produce a refractory residue and it is relevant for comets and trans-Neptunian objects (Strazzulla & Johnson 1991; Baratta et al. 2019). The fluence used in UV irradiation experiments (2×10^{19} photons cm^{-2}) is of the same order as the highest fluence suffered by icy grain mantles in dense molecular clouds. In this view, our experiments show that the refractory organic material observed in meteorites, IDPs, and cometary dust particles could have been formed either in the protostellar phase or in the solar system.

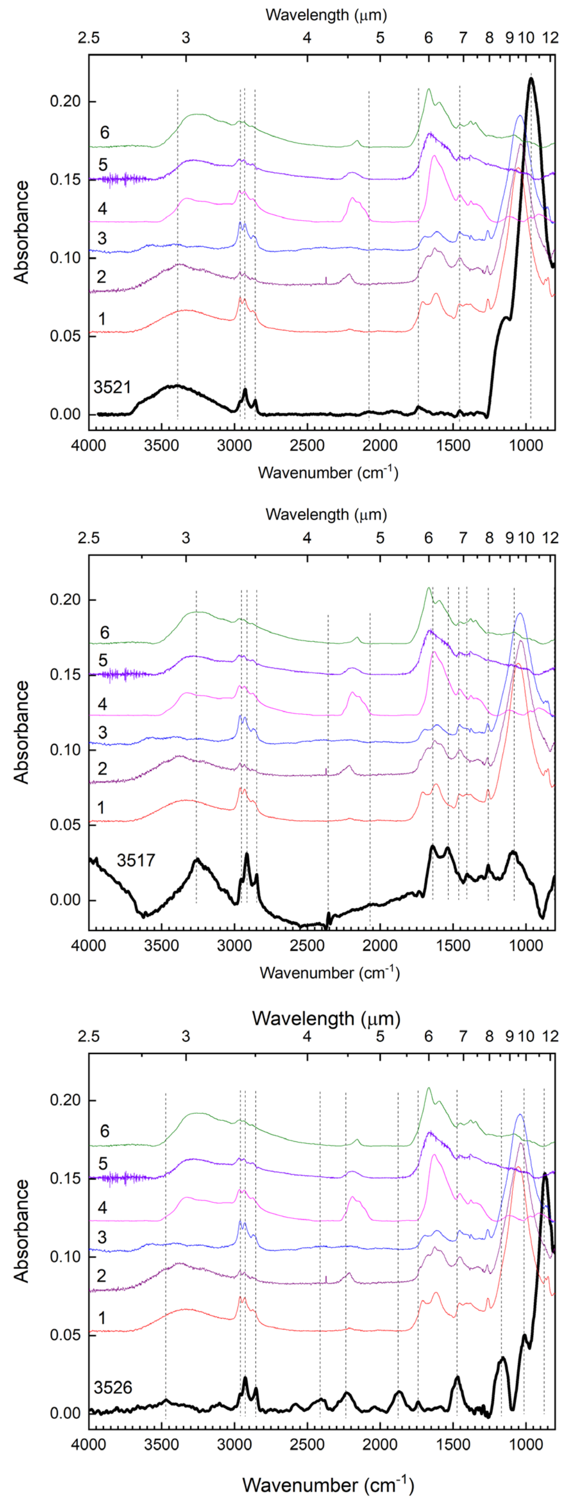

Figure 4. Comparison of the absorption spectra of Stardust particles 3521 (upper), 3517 (middle), and 3526 (lower) and the laboratory organic residues produced in Jena and Catania from N-containing ice mixtures (mentioned in the figure). The spectra are vertically shifted for clarity. The original spectra of particles 3521 and 3526 are divided by 10. The vertical dashed lines indicate the most prominent absorption features in the particle spectra. Ice mixtures: (1) H_2O:CH_3OH:NH_3 (UV irradiation, Jena), (2) H_2O:CO_2:NH_3 (UV irradiation, Jena), (3) H_2O:CH_4:NH_3 (UV irradiation, Jena), (4) N_2:CH_4 (ion irradiation, Catania), (5) N_2:CH_4:CO (ion irradiation, Catania), and (6) N_2:CH_4:H_2O (ion irradiation, Catania).

4.2. Formation Location of the Extraterrestrial Particles

Due to the spectral signatures of the meteorites, IDPs, and Stardust particles in the region of 3750–3000 cm^{-1}, where

Table 4
IR Bands (cm^{-1}) of the Stardust Particles and Their Attributions

3521	3517	3526	Band Attributions
3750–3000 (p)	3600–3000 (p)	3750–3200 (p) + 3200–3020	OH stretching, NH, NH_2 stretching
2955 (p), 3924 (p)	2960 (p), 2925 (p)	2960 (p), 2925 (p)	CH stretching (asym; Colangeli et al. 1995)
2854	2854 (p)	2854 (p)	CH stretching (sym; Colangeli et al. 1995)
...	...	2582	?
...	...	2410 (p)	?
...	2356 (p)	...	?
...	2310	...	?
2150–2010 (p)	2120–2000 (p)	2320–2120 (p)	C ≡ N stretching (Accolla et al. 2018)
1910	...	...	?
...	...	1870 (p)	?
...	1788	...	?
1739 (p), 1667, 1580	1730, 1638 (p)	1740 (p), 1610, 1585	C = O, C = C, C = N stretching (Munoz Caro & Schutte 2003), HOH bending, NH_2 bending (Accolla et al. 2018)
...	1537 (p)	...	CO_3^{2-} stretching (Aguiar et al. 2009; Ciaravella et al. 2018)
1454 (p)	1466 (p), 1450	1470 (p)	CH bending (Munoz Caro & Schutte 2003; Jäger et al. 2008)
...	1406 (p)	...	CO_3^{2-} stretching (Aguiar et al. 2009; Ciaravella et al. 2018)
1378	1375	...	CH bending (Colangeli et al. 1995; Jäger et al. 2008)
...	1307	...	COO^- stretching (sym; Munoz Caro & Schutte 2003)
...	1260 (p)	...	?
...	1232	...	?
...	...	...	?
1170	...	1160 (p)	S–O stretching
962 (p)	1084 (p), 1020, 950	1010 (p)	SiO stretching[a]
...	...	872 (p)	out-of-plane CH bending (Colangeli et al. 1995; Jäger et al. 2008)
812	805 (p)	...	?

Note. The band positions are determined in this study. The notation (p) indicates the most prominent absorption features shown in Figure 4.
[a] The profile of the silicate band is due to the contribution given by the silicate in the particle as well as by the silica aerogel.

trapped water is detected in the Jena samples, we conclude that trapped water is probably present in the extraterrestrial particles. Note that trapped water originates from ice/silicate mixtures at low temperatures and its formation does not require high-temperature processing as in the case of hydrated silicates (phyllosilicates), where OH groups or H_2O molecules are chemically incorporated into crystalline silicates. Thus, the formation of trapped water is relevant to both meteorites and comets formed in low-temperature regions beyond the water snowline.

This conclusion is reinforced by the detection of the C ≡ N triple bond in the IDPs and Stardust particles meaning that N-bearing species were present in the particle material at the formation of the organic residue. This indicates that comets originate in the outer regions of the solar nebula, beyond the snowline of one of the most abundant N-bearing species in cometary ices , nitrogen (snowline at about 40 K) and ammonia (snowline at about 100 K). The nondetection of the C ≡ N bond in the meteorite spectra (see Figure 2 and Table 3) reinforces this conclusion as meteorites are derived from asteroids formed in the region between 2 and 4 au, at temperatures much higher than 100 K. This result is in line with the finding of nitrogen-rich organic matter in ultracarbonaceous micrometeorites recovered from Antarctica (representing a small fraction of IDPs reaching the Earth's surface), which has also been referred to the formation location of organic matter in low-temperature regions of the solar system (Dartois et al. 2013, 2018).

Recent literature on comets agrees with the fact that comets' organics come from the interplanetary medium (Raponi et al. 2020). However, we want to note that several authors have proposed that organic compounds could be formed in the envelopes of evolved stars and delivered through the ISM to our environment (Papoular 2001; Kwok & Zhang 2011; Endo et al. 2021). The formation of –CN groups (nitrile or cyanide groups) is observed in gas-phase condensation processes

Table 5
Comparison of the Ion and UV Fluxes and Doses in Different Astrophysical Environments

Environment	Time	Energetic Ions		UV Photons			Reference
	(yr)	Flux (ions cm^{-2} s^{-1})	Dose (eV/molecule)	Flux (photons cm^{-2} s^{-1})	Dose (eV/molecule)	Fluence (photons cm^{-2})	
Diffuse interstellar clouds	10^7	10	30	9.6×10^7	10^6	3×10^{22}	(Moore 1999)
Dense molecular clouds	10^7	1	1–10	2×10^3–3×10^4	10–100	6×10^{17}–9×10^{18}	(Shen et al. 2004)
T Tauri disks (500 au)	10^6	8×10^4	2.4×10^4	2.9×10^{10}	2.9×10^7	9×10^{23}	(Strazzulla et al. 1983; Pedersen & Gomez de Castro 2011)
Cometary nuclei (Oort cloud)	10^9	10	600 (down to a depth of a few meters)	10^3–10^5	10^3–10^5 (down to a depth of a few hundred nanometers)	3×10^{19}–3×10^{21}	(Strazzulla & Johnson 1991; Modica et al. 2012)

performed in molecular nitrogen. It is generally known that the condensation of carbon particles in a nitrogen atmosphere forms a big amount of nitriles in the carbon structure. The incorporation of nitrogen (in the form of nitrile groups) into refractory carbonaceous matter is efficient. The use of NH_3 is less efficient for nitrile formation (Alexandrescu et al. 1998; Thareja et al. 2002). Consequently, circumstellar envelopes around late-type stars can produce carbonaceous grains containing nitriles. A top-down synthesis of carbonaceous matter or molecules containing nitriles or other nitrogen-bearing molecules from circumstellar dust could be possible. However, this idea needs further investigation. For now, there is no convincing evidence for such a scenario.

Detection of vibrational signatures of carbonate groups related to amorphous magnesium carbonate in combination with the formation of extraterrestrial particles beyond the nitrogen or ammonia snowline speaks to their formation in cold regions (the outer solar nebula or its parent ISM). To clarify the origin of carbonates, they should be searched for in diffuse and dense interstellar clouds. The James Webb Space Telescope (JWST) may provide a sensitivity high enough for the detection of carbonates in the ISM.

4.3. Origin of Water on Earth and Other Terrestrial Planets

Detection of trapped water in extraterrestrial particles (some of which have reached Earth) is linked to another intriguing question—could the building blocks of Earth have been wet? Assuming that solid-state water exists only beyond the water snowline in planet-forming disks, two scenarios for the delivery of water to the surface of terrestrial planets have been proposed (van Dishoeck et al. 2014). In the so-called dry scenario, the planets are initially built up from planetesimals/pebbles inside the snowline with low (or no) water mass fractions, and water is delivered to their surfaces by water-rich asteroids formed outside the snowline. Alternatively, in the so-called wet scenario, the planets either accreted a water-rich atmosphere or formed beyond the snowline. For instance, in the pebble accretion scenario, the pebbles that form planets drift inward from the outer disk regions, carrying water ice with them. The ice evaporates resulting in water vapor diffusing into the inner disk (Bitsch et al. 2021).

However, one more possibility for the wet scenario is that local planetesimals/pebbles at the time of the Earth's formation retained some water at high temperatures through its physisorption or chemisorption on silicate grains. This is exactly the phenomenon that we observe in the laboratory—trapped water on silicates. In the present study, we provide evidence for the presence of trapped water in comets and meteorites. Such objects could have delivered water to the early Earth.

A search for water trapped on silicates in the inner regions (inside the H_2O snowline) of planet-forming disks should be also possible with JWST and may shed light on the origin of water on Earth and other terrestrial planets (and, potentially, on extrasolar planets). Appropriate observations are on the horizon.

We thank Hope Ishii for providing the IDP U217B19 data and Torsten Löhne for providing the values for stellar UV fluxes. A.P. and C.J. acknowledge support from Research Unit FOR 2285 "Debris Disks in Planetary Systems" of Deutsche Forschungsgemeinschaft (grant JA 2107/3-2). M.E.P. acknowledges the support of the Italian Ministero dell'Istruzione, dell'Università e della Ricerca through the grant Progetti Premiali 2012-iALMA. G.B. acknowledges financial support from the Italian Space Agency (ASI) contract No. 2013-073-R.0: PSS (Photochemistry on the Space Station). T.H. acknowledges support from the European Research Council (ERC) under the Horizon 2020 Framework Program via the ERC Advanced Grant Origins 83 24 28.

ORCID iDs

Alexey Potapov https://orcid.org/0000-0002-3699-7477
Maria Elisabetta Palumbo https://orcid.org/0000-0002-9122-491X
Zelia Dionnet https://orcid.org/0000-0002-3679-6333
Andrea Longobardo https://orcid.org/0000-0002-1797-2741
Cornelia Jäger https://orcid.org/0000-0001-7803-0013
Giuseppe Baratta https://orcid.org/0000-0002-3688-160X
Alessandra Rotundi https://orcid.org/0000-0001-5467-157X
Thomas Henning https://orcid.org/0000-0002-1493-300X

References

Accolla, M., Pellegrino, G., Baratta, G. A., et al. 2018, A&A, 620, A123
Aguiar, H., Serra, J., Gonzalez, P., & Leon, B. 2009, JNCS, 355, 475
Aléon-Toppani, A., Brunetto, R., Aléon, J., et al. 2021, M&PS, 56, 1151
Alexandrescu, R., Cojocaru, S., Crunteanu, A., et al. 1998, Carbon, 36, 795
Altwegg, K., Balsiger, H., Bar-Nun, A., et al. 2016, SciA, 2, e1600285
Baratta, G. A., Accolla, M., Chaput, D., et al. 2019, AsBio, 19, 1018
Baratta, G. A., Chaput, D., Cottin, H., et al. 2015, P&SS, 118, 211
Baratta, G. A., Leto, G., & Palumbo, M. E. 2002, A&A, 384, 343
Bernstein, M. P., Dworkin, J. P., Sandford, S. A., Cooper, G. W., & Allamandola, L. J. 2002, Natur, 416, 401
Bernstein, M. P., Sandford, S. A., Allamandola, L. J., Chang, S., & Scharberg, M. A. 1995, ApJ, 454, 327
Bitsch, B., Raymond, S. N., Buchhave, L. A., et al. 2021, A&A, 649, L5
Boogert, A. C. A., Gerakines, P. A., & Whittet, D. C. B. 2015, ARA&A, 53, 541
Brack, A. 1999, AdSpR, 24, 417
Bradley, J. P. 2003, TrGeo, 1, 689
Brunetto, R., Borg, J., Dartois, E., et al. 2011, Icar, 212, 896
Caselli, P., & Ceccarelli, C. 2012, A&ARv, 20, 56
Chyba, C., & Sagan, C. 1992, Natur, 355, 125
Ciaravella, A., Jimenez-Escobar, A., Cosentino, G., et al. 2018, ApJ, 858, 35
Cobb, A. K., & Pudritz, R. E. 2014, ApJ, 783, 140
Colangeli, L., Mennella, V., Bussoletti, E., et al. 1995, P&SS, 43, 1263
Cooper, G., Kimmich, N., Belisle, W., et al. 2001, Natur, 414, 879
Cronin, J. R., & Chang, S. 1993, in NATO ASI Series C, 416, Chemistry of Life's Origins, ed. J. M. Greenberg, V. Pirronello, & C. Mendoza-Gomez (Dordrecht: Springer), 209
Cruz-Diaz, G. A., Munoz Caro, G. M., Chen, Y. J., & Yih, T. S. 2014a, A&A, 562, A119
Cruz-Diaz, G. A., Munoz Caro, G. M., Chen, Y. J., & Yih, T. S. 2014b, A&A, 562, A120
d'Hendecourt, L. B., & Allamandola, L. J. 1986, A&AS, 64, 453
Dartois, E., Engrand, C., Brunetto, R., et al. 2013, Icar, 224, 243
Dartois, E., Engrand, C., Duprat, J., et al. 2018, A&A, 609, A65
Dionnet, Z., Aleon-Toppani, A., Baklouti, D., et al. 2018, M&PS, 53, 2608
Ehrenfreund, P., & Charnley, S. B. 2000, ARA&A, 38, 427
Elsila, J. E., Dworkin, J. P., Bernstein, M. P., Martin, M. P., & Sandford, S. A. 2007, ApJ, 660, 911
Elsila, J. E., Glavin, D. P., & Dworkin, J. P. 2009, M&PS, 44, 1323
Endo, I., Sakon, I., Onaka, T., et al. 2021, ApJ, 917, 103
Fanchini, G., Messina, G., Paoletti, A., et al. 2002, Surf. Coat. Technol., 151, 257
Ferini, G., Baratta, G. A., & Palumbo, M. E. 2004, A&A, 414, 757
Fresneau, A., Abou Mrad, N., d'Hendecourt, L. L. S., et al. 2017, ApJ, 837, 168
Gerakines, P. A., Schutte, W. A., Greenberg, J. M., & van Dishoeck, E. F. 1995, A&A, 296, 810
Goesmann, F., Rosenbauer, H., Bredehoft, J. H., et al. 2015, Sci, 349, aab0689
Greenberg, J. M., Li, A., Mendozagomez, C. X., et al. 1995, ApJL, 455, L177
Hammer, P., Lacerda, R. G., Droppa, R., & Alvarez, F. 2000, DRM, 9, 577

Henning, T., & Semenov, D. 2013, ChRv, 113, 9016
Hewins, R. H., Bourot-Denise, M., Zanda, B., et al. 2014, GeCoA, 124, 190
Hudgins, D. M., Sandford, S. A., Allamandola, L. J., & Tielens, A. G. G. M. 1993, ApJS, 86, 713
Hudson, R. L., & Moore, M. H. 2002, ApJ, 568, 1095
Hudson, R. L., Moore, M. H., Dworkin, J. P., Martin, M. P., & Pozun, Z. D. 2008, AsBio, 8, 771
Ishii, H. A., Bradley, J. P., Bechtel, H. A., et al. 2018, PNAS, 115, 6608
Islam, F., Baratta, G. A., & Palumbo, M. E. 2014, A&A, 561, A73
Jäger, C., Mutschke, H., Henning, T., & Huisken, F. 2008, ApJ, 689, 249
Keller, L. P., Bajt, S., Baratta, G. A., et al. 2006, Sci, 314, 1728
Kobayashi, K., Ogawa, T., Tonishi, H., et al. 2008, Electron. Commun. Jpn., 91, 15
Krasnokutski, S. A., Chuang, K. J., Jager, C., Ueberschaar, N., & Henning, T. 2022, NatAs, 6, 381
Krasnokutski, S. A., Jäger, C., & Henning, T. 2020, ApJ, 889, 67
Kwok, S., & Zhang, Y. 2011, Natur, 479, 80
Mackinnon, I. D. R., & Rietmeijer, F. J. M. 1987, RvGeo, 25, 1527
Materese, C. K., Cruikshank, D. P., Sandford, S. A., et al. 2014, ApJ, 788, 111
Matrajt, G., Borg, J., Raynal, P. I., et al. 2004, A&A, 416, 983
Matthewman, R., Martins, Z., & Sephton, M. A. 2013, AsBio, 13, 324
Meinert, C., Myrgorodska, I., de Marcellus, P., et al. 2016, Sci, 352, 208
Mennella, V., Baratta, G. A., Esposito, A., Ferini, G., & Pendleton, Y. J. 2003, ApJ, 587, 727
Merouane, S., Djouadi, Z., & d'Hendecourt, L. L. S. 2014, ApJ, 780, 174
Modica, P., Palumbo, M. E., & Strazzulla, G. 2012, P&SS, 73, 425
Moore, M. H. 1999, in Solid Interstellar Matter: the ISO Revolution, ed. L. d'Hendecourt, C. Joblin, & A. Jones (New York: Springer), 199
Munoz Caro, G. M., Ciaravella, A., Jimenez-Escobar, A., et al. 2019, ESC, 3, 2138
Munoz Caro, G. M., Dartois, E., Boduch, P., et al. 2014, A&A, 566, A93
Muñoz Caro, G. M., Meierhenrich, U. J., Schutte, W. A., et al. 2002, Natur, 416, 403
Munoz Caro, G. M., & Schutte, W. A. 2003, A&A, 412, 121
Nuevo, M., Meierhenrich, U. J., Muñoz Caro, G. M., et al. 2006, A&A, 457, 741
Nuevo, M., Milam, S. N., & Sandford, S. A. 2012, AsBio, 12, 295
Oba, Y., Kimura, T., Hayashi, M., & Yamamoto, K. 2022, MaMol, 55, 1771
Oba, Y., Takano, Y., Naraoka, H., Watanabe, N., & Kouchi, A. 2019, NatCo, 10, 4413
Oba, Y., Takano, Y., Watanabe, N., & Kouchi, A. 2016, ApJL, 827, L18
Oro, J. 1961, Natur, 190, 389
Osawa, T., Hirao, N., Takeda, N., & Baba, Y. 2009, EP&S, 61, 1003
Palumbo, M. E., Ferini, G., & Baratta, G. A. 2004, AdSpR, 33, 49
Papoular, R. 2001, A&A, 378, 597
Pearce, B. K. D., Pudritz, R. E., Semenov, D. A., & Henning, T. K. 2017, PNAS, 114, 11327
Pedersen, A., & Gomez de Castro, A. I. 2011, ApJ, 740, 77
Poch, O., Istiqomah, I., Quirico, E., et al. 2020, Sci, 367, aaw7462
Potapov, A., Bouwman, J., Jäger, C., & Henning, T. 2021, NatAs, 5, 78
Potapov, A., Fulvio, D., Krasnokutski, S., Jäger, C., & Henning, T. 2022, JPCA, 126, 1627
Potapov, A., Jäger, C., & Henning, T. 2018a, ApJ, 865, 58
Potapov, A., Mutschke, H., Seeber, P., Henning, T., & Jäger, C. 2018b, ApJ, 861, 84
Prasad, S. S., & Tarafdar, S. P. 1983, ApJ, 267, 603
Quirico, E., Montagnac, G., Lees, V., et al. 2008, Icar, 198, 218
Raponi, A., Ciarniello, M., Capaccioni, F., et al. 2020, NatAs, 4, 500
Rodil, S. E. 2005, DRM, 14, 1262
Rotundi, A., Baratta, G. A., Borg, J., et al. 2008, M&PS, 43, 367
Rotundi, A., Rietmeijer, F. J. M., Ferrari, M., et al. 2014, M&PS, 49, 550
Rubin, A. E., Trigo-Rodriguez, J. M., Huber, H., & Wasson, J. T. 2007, GeCoA, 71, 2361
Sabri, T., Gavilan, L., Jager, C., et al. 2014, ApJ, 780, 180
Sandford, S. A., Aleon, J., Alexander, C. M. O'D., et al. 2006, Sci, 314, 1720
Sandford, S. A., & Bradley, J. P. 1989, Icar, 82, 146
Sandford, S. A., Nuevo, M., Bera, P. P., & Lee, T. J. 2020, ChRv, 120, 4616
Shen, C. J., Greenberg, J. M., Schutte, W. A., & van Dishoeck, E. F. 2004, A&A, 415, 203
Strazzulla, G., & Johnson, R. E. 1991, IAU Colloq. 116, Comets in the post-Halley era (Dordrecht: Kluwer), 243
Strazzulla, G., Pirronello, V., & Foti, G. 1983, ApJ, 271, 255
Tachibana, S., Kouchi, A., Hama, T., et al. 2017, SciA, 3, eaao2538
Thareja, R. K., Dwivedi, R. K., & Ebihara, K. 2002, NIMPB, 192, 301
Urso, R. G., Scire, C., Baratta, G. A., Compagnini, G., & Palumbo, M. E. 2016, A&A, 594, A80
Urso, R. G., Vuitton, V., Danger, G., et al. 2020, A&A, 644, A115
van Dishoeck, E. F., Bergin, E. A., Lis, D. C., & Lunine, J. I. 2014, in Protostars and Planets VI, ed. H. Beuther et al. (Tucson, AZ: Univ. of Arizona Press), doi:10.2458/azu_uapress_9780816531240-ch036
Westley, M. S., Baragiola, R. A., Johnson, R. E., & Baratta, G. A. 1995, Natur, 373, 405
Wooden, D. H., Ishii, H. A., & Zolensky, M. E. 2017, RSPTA, 375, 20160260
Wu, Y. J., Wu, C. Y. R., Chou, S. L., et al. 2012, ApJ, 746, 175